Climate Dynamics (2000) 16:701–717 © Springer-Verlag 2000

H. Grenier · H. Le Treut · T. Fichefet

Ocean-atmosphere interactions and climate drift in a coupled general circulation model

Received: 8 December 1998 / Accepted: 6 January 2000

Abstract We have analysed numerical simulations performed with a global 3D coupled atmosphere-ocean model to focus on the role of atmospheric processes leading to sea surface temperature (SST) drift in the tropics. Negative SST errors occur coherently in space and time with large positive errors in latent heat and momentum fluxes at the tropical air-sea interface, as diagnosed from forced SST simulations. The warm pool in the western Pacific disappears after a few years of simulation. Strong SST gradients enforce regions of high precipitation that are thin and stationary north of the equator. We detail the implications for the ocean-atmosphere system of such upheaval in the deep convection location. A sensitivity experiment to empirically formulate air-sea drag coefficient shows that the rapid warm pool erosion is not sensitive to changes in the formulation of the surface drag coefficient over the oceans because the corresponding changes in turbulent heat fluxes and LW cooling approximately cancel one another. In the eastern Pacific, the improvement in SST is striking and caused by feedbacks between SST, surface turbulent fluxes and boundary layer cloud fraction, which decreases as SST warms.

1 Introduction

Large-scale atmospheric dynamics, convective and turbulent motions, radiative processes and energy exchanges between the atmosphere and the underlying surface, all contribute to determine the mean climate of the Earth and its sensitivity to perturbations. These processes, however, interact in a strongly non-linear manner. Problems faced by 3D coupled atmosphere-ocean general circulation models (AOGCM) to reproduce the observed climate statistics faithfully (Meehl 1995), are testimonies to this complexity. Roughly half of the models participating in the Coupled Model Intercomparison Project (CMIP) still use flux-correction methods to yield a stable climate, whereas many other models have to tune the top-of-the-atmosphere (TOA) radiative balance through adjustments in model parameters. Even so, the SST distributions simulated by these complex climate models rarely reproduce the observed distribution accurately. Apart from the case where the coupled model surface energy and/or water budget is corrected from imbalances between the atmospheric and oceanic models surface budget (Sausen et al. 1988), it seems inevitable that the sea surface temperature field simulated by three-dimensional coupled models, especially at low resolution, departs from the mean climatological SST field (Weaver and Hughes 1996). Reducing the SST bias is a long-term effort, which may be eased if the mechanisms responsible for the SST drift are properly identified. Our main purpose is to describe our approach to understand and reduce the drift in tropical SST simulated by a global, coupled and low resolution 3D climate model. Naturally related to this issue, is the problem of the stability of tropical SSTs in the real climate: what are the processes which control the tropical climate stability? Some process studies conducted with coupled atmosphere-ocean models have been specifically dedicated to address this issue. They examined the importance of the following non-linear mechanisms: the low-level stratus clouds and the tropical Pacific circulation (Ma et al. 1996; Philander et al. 1996), the tropical cirrus cloud feedback (Meehl and Washington 1995), and the thermostat oceanic feedback (Clement et al. 1996), in controlling the SST in the tropics. The study by Ma et al. (1994) concludes that the climate sensitivity to atmospheric parametrisations is

H. Grenier[1] (✉) · T. Fichefet
Institut d'Astronomie et de Géophysique G. Lemaître,
Université Catholique de Louvain, Louvain-la-Neuve, Belgium

H. Le Treut
Laboratoire de Météorologie Dynamique du CNRS,
Ecole Normale Supérieure, Paris, France

[1] *Present address*:
Department of Atmospheric Sciences,
University of Washington, Box 351640, Seattle,
WA 98195-1640, USA

drastically different in forced and coupled modes, because of the importance of air-sea interactions. Terray (1998) has shown that the tropical climate simulated by his coupled model is very sensitive to uncertain atmospheric parameters, such as the entrainment rate in the cumulus cloud model, or the relative humidity threshold for condensation used in the cloud cover computation. Despite their obvious diversity, it appears from these studies that it is through the hydrological cycle, and the interactions between radiation, convective motions and large-scale dynamics that the sensitivity of the tropical climate to parametrised atmospheric processes is effective. Not surprisingly, improving our understanding of these interplaying processes is a current and open area of research (e.g. Larson et al. 1999). The present work represents an attempt to verify whether a 3D coupled atmosphere-ocean model, of low resolution, can be successfully used to address the question of ocean-atmosphere interactions in the tropics, in particular, those related to the role of water vapour (Hartman and Michelsen 1993; Pierrehumbert 1995; Spencer and Braswell 1997; Soden 1997). We use the initial instability of this newly built coupled model to diagnose the dominant processes responsible for changes in the tropical climate dynamics. Later, we address the role of dynamical adjustments of the atmospheric circulation, which can impact the longitudinal structure of the convection and the associated heat sources, in particular radiative heat sources.

2 Model description and performances

In this section, we describe the two components of our coupled climate model and discuss some of the atmospheric model weaknesses inferred from a simulation performed with prescribed SSTs and sea ice distribution.

2.1 The atmospheric model and its performance in uncoupled mode

The atmospheric model is version 5.2 of the Laboratoire de Météorologie Dynamique (LMD) General Circulation Model (AGCM) (Le Treut et al. 1994). This model is a grid point model whose main features, in particular the discretisation over an Arakawa C-grid, are described in a seminal paper by Sadourny and Laval (1984). For all the experiments presented here, a low resolution (64 points in longitude $\times$ 50 points in latitude $\times$ 11 vertical levels) has been used both in forced and coupled mode. In the following, we briefly review some of the parametrisations most relevant to this study.

The radiative transfer schemes are similar to those used in the European Center for Medium Range Weather Forecast (ECMWF) model. In the longwave domain (LW), it is due to Morcrette (1991). Trace gases other than CO_2 are not explicitly included in the computation of the absorption/emission of atmospheric layers. In the solar spectrum, a version of the code proposed by Fouquart and Bonnel (1980) is used. The solar diurnal cycle and the presence of aerosols are not accounted for in the simulations presented henceforth. Convection is represented by Manabe's moist adjustment scheme (Manabe et al. 1965) which removes conditional instability, and a modified version of Kuo scheme (Kuo 1965), triggered by convergence of water vapour in the planetary boundary layer (PBL). These convective schemes provide tendencies for temperature and total water content.

The water condensed during the convective adjustment process is treated jointly with the vapour phase in a statistical cloud scheme which solves for the cloud fraction and condensate mixing ratio (Le Treut and Li 1988). Ad-hoc assumptions are used to define the distribution function of total water within a grid box. Le Treut and Li (1988) chose a simple top-hat distribution of total water centred around the mean grid box value. The width of the distribution was specified such as to allow condensation to occur at a critical relative humidity of 83%. Recently, Xu and Randall (1996) discussed the validity of such statistical schemes, arguing that a single probability distribution function does not allow for the description of the wide variety of cloud regimes occurring within the atmosphere. In order to account for dependency of cloud regimes on large-scale conditions as discussed by Xu and Randall (1996), we have made the width of the top-hat distribution a prescribed function of the altitude, implicitely taking into account the correlation between the cloudiness regime, the PBL depth and the total water variance: stratocumulus (respectively cumulus) convection is correlated with low values (respectively high values) of total water variance, and is more likely to occur in a shallow PBL than in a deep PBL. This modification in the cloud scheme is performed simultaneously with changes in the computation of the mixing coefficient across the inversion along the following lines. Entrainment is not explicitly computed. Instead, a small value of the eddy diffusivity crudely controls the turbulent fluxes at the top of the PBL. Such a formulation does not follow the physical rules which govern entrainment across PBL top, but is still of general use in AGCM which a crude multi-layer PBL representation. From preliminary experiments, we had found that the inversion was too weak and its relative humidity well below 100% in regions where stratocumulus (Sc) convection is expected to occur. In an ad-hoc manner, we have lowered the minimum value allowed for eddy diffusivities across a stable layer from 10^{-2} to 10^{-4} m^2 s^{-1}. In this AGCM, this has the virtue of greatly improving the seasonal cycle of the boundary layer cloudiness over the tropical eastern oceanic basins, and over the extra-tropical oceans in summer. However, the model still suffers from systematic errors in the vertical structure of the cloudy boundary layer.

The prognostic equation for water condensate does not distinguish between its liquid and solid phase. But it is assumed that the condensate precipitated out of an atmospheric cell is made of solid, liquid, or mixed phases, depending on the temperature of the cell. Temperature thresholds for this highly idealised treatment of the Bergeron process are fixed at -15 °C and -5 °C (Le Treut et al. 1994). Radiative properties of clouds are computed interactively from diagnosed liquid water path and cloud temperature (Le Treut et al. 1994). Some parameters have to be specified in order to compute the optical thickness of clouds and their emissivity. These important parameters for the planetary budget include the effective radius of water clouds (12 μm), ice clouds (40 μm) and the absorption coefficient of cold and warm clouds which take respectively the values of 0.08 and 0.13 m^2/g. At the surface, turbulent fluxes of heat and momentum are computed using bulk aerodynamic formulae, which require the evaluation of the drag coefficient at the surface, C_d. Bunker (1979) synthesised data obtained from ship measurements over the North Atlantic to compute polynomial functions which relate C_d to the near surface static stability and wind shear. These polynomial functions are used in the control (forced and coupled) experiments to compute the drag coefficient at the air-sea interface. A more common way to compute C_d from grid point model variables is to parametrise it as the product of a neutral drag coefficient involving a length scale z_0 (the roughness length of the surface), and stability functions correcting for convective versus stable situations, and involving the Monin-Obukhov length. Louis et al. (1981) derived such stability functions for use in large-scale models of the atmosphere, which only involve the computation of a near-surface bulk Richardson number. A sensitivity experiment using Louis et al.'s (1981) formulation instead of Bunker's (1979) one is described in Sect. 4. Above the surface layer, vertical eddy diffusivities and viscosities are computed using a mixing length profile and a diagnostic of the turbulent kinetic energy given by a bulk Richardson number. Shallow convection is not

explicitely dealt with. Two other important processes parametrised in the LMD AGCM are the hydrologic and energetic exchanges between the soil-vegetation system and the atmosphere (Ducoudré et al. 1992) and the momentum deposition by vertically propagating gravity waves in the upper troposphere and lower stratosphere (Boer et al. 1984).

A three year duration experiment has been conducted with this AGCM in order to evaluate its overall performance in uncoupled mode. In this simulation, the model was forced by daily averaged insolation at the top-of-the-atmosphere, and by daily observed SSTs and sea-ice distribution, representative of the mean climatological state of the ocean-atmosphere interface for the period 1978 to 1987. This experiment is hereafter referred to as the F_{CONT} simulation. The ability of the similar LMD5.3 model to simulate the natural variability of the climate was discussed extensively by Harzallah and Sadourny (1995). Here, we analyse the F_{CONT} simulation in terms of surface turbulent fluxes of heat and momentum, outgoing longwave radiation (OLR) at the top-of-the-atmosphere, and moisture content in the tropical atmosphere.

The map of differences between the simulated annual mean water fluxes at the air-sea interface and those from the da Silva et al. (1995) analysis (from the Coarse Ocean Atmosphere Data Set, hereafter COADS) (Fig. 1) shows that both the evaporation and the precipitation are largely overestimated by the AGCM. The bias in the evaporation flux is uniformly distributed over the whole tropical oceans, it exceeds 2 mm of water per day over large regions. The precipitation error is less spatially homogeneous and can reach 3 mm per day locally. Departures between the simulation and observations are generally larger than the uncertainty within the observational data set, as estimated by Gleckler and Weare (1996). Both the zonal and meridional components of the surface wind stress are too intense over the Pacific and Atlantic Oceans (Fig. 2). In the southern tropical regions, the westward wind stress is positively biased by 50%. Over the western Pacific warm pool, surface friction should be small, as can be seen in the COADS data set, because the flow is strongly convergent at the annual time scale (Zhang et al. 1995). The AGCM fails to reproduce this trade-wind weakening associated with the climatological Inter Tropical Convergence Zone (ITCZ) and therefore, zonal wind stress anomalies remain large, from the central Pacific to the Indonesian Archipelago. Errors in the surface friction and errors in the western Pacific precipitation patterns are likely to be strongly related (Zhang et al. 1995). One also notes that along coastlines, the wind stress is poorly simulated. The simulated atmospheric flow is large and toward the shore near most of the tropical western coastlines, while in the observed system, its magnitude is small and its direction modulated by the seasonal cycle (Mitchell and Wallace 1992).

The simulated annual mean vertically integrated water vapour content (Fig. 3) presents negative biases when compared to the satellite estimates after the algorithm of Wentz (1983). These biases reach 10 kg/m^2 over the western Pacific warm pool, which represents 20% of the satellite-retrieved water vapour content. Such tropospheric dryness, simultaneous with positive biases in precipitation and evaporation, means that the model hydrological cycle is too intense. This problem may have several origins, among which the deep convection scheme, the conversion rate of condensate to precipitation, the absence of explicit representation of shallow convection are tentative candidates. Consistently with the dry troposphere, the tropospheric temperature field shows cold biases with respect to the observations (not shown). In the zonal mean, the cold bias increases slightly from the boundary layer to 700 hPa, where it reaches 5°, and then remains roughly constant up to the tropopause. As discussed by Johnson (1997), this property is common to many AGCMs, although it is accentuated here.

OLR diagnostics show positive biases in the model, which indicate that the overestimated latent heating is accompanied by excessive radiative loss to space (see Fig. 4). OLR maxima over the subtropical regions are biased by 10 to 20 Wm^{-2} in the zonal mean compared to ERBE (Earth Radiation Budget Experiment) data (Barkstrom and Smith 1986). OLR minima in the moist regions of the tropics are underestimated by a similar quantity. One finally notes a bias in the position of the OLR minimum, indicating that despite SSTs are imposed, the geographical alternation of dry and moist zones is only approximately captured by the model.

In summary, the important discrepancies between the simulation and the observations tend to indicate that the hydrological cycle is mis-represented. This has important impacts on the LW planetary budget.

2.2 The oceanic model and coupling procedure

The ocean-sea ice model is the CLIO (Coupled Large-scale Ice-Ocean) model developped at the Université Catholique de Louvain

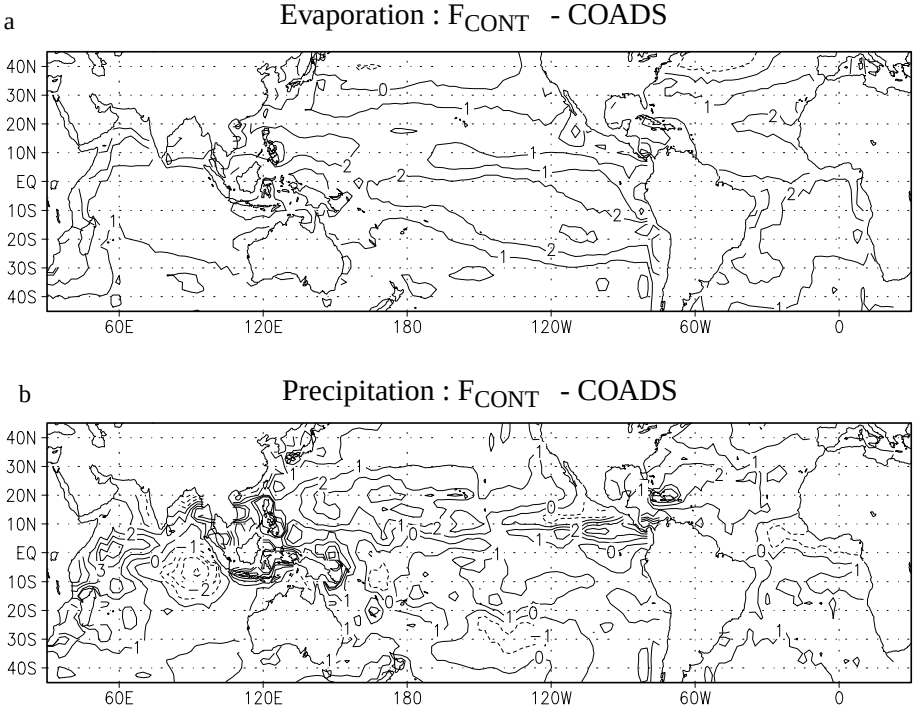

Fig. 1a, b Differences of annual mean surface **a** evaporation and **b** precipitation between experiments F_{CONT} and COADS data (da Silva et al. 1995). Units are mm/day

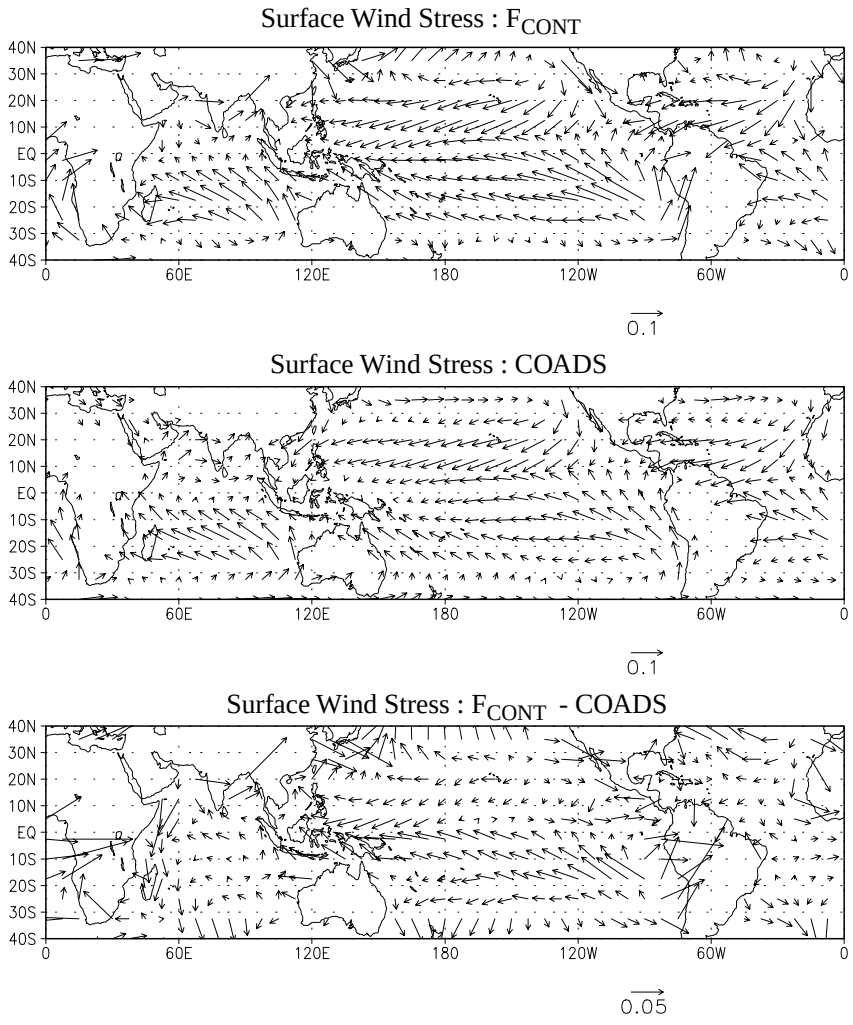

Fig. 2a–c Annual mean surface wind stress as simulated **a** in F_{CONT}, **b** as computed by da Silva et al. (1995), and **c** difference F_{CONT} − COADS . Units are Nm^{-2}

(UCL) (Goosse et al. 1997a, b). To cope with the singularity at the North Pole associated with the geographical spherical coordinates, two spherical grids connected in the equatorial Atlantic are used: a grid with its poles on the geographical equator for the North Alantic and the Arctic, and a normal latitude-longitude grid for the rest of the domain. This model is made up of a primitive equation, free-surface ocean general circulation model (Deleersnijder and Campin 1995), coupled to a thermodynamic-dynamic sea ice model with viscous-plastic rheology (Fichefet and Morales Maqueda 1997). Vertical mixing is computed according to the parametrisation of Pacanowski and Philander (1981), and the effect of mesoscale eddies is crudely represented by a classical horizontal diffusion scheme. The horizontal resolution is of $3° \times 3°$, and there are 20 unevenly spaced vertical levels in the ocean. In this work, we focus on atmosphere-ocean interaction processes in the tropics, and refer to Goosse et al. (1997a, b) for the description of the model ability to reproduce the oceanic circulation.

The spin-up procedure was the following. The model was first integrated for 20 years in robust diagnostic mode (i.e., with interior restoring to the annual mean Levitus 1982 temperatures and salinities on a 1 year time scale), from a state of rest. The relaxation was then suppressed, except in the uppermost grid box for salinity, and the integration was pursued for 450 years. During this phase, the ocean was driven by surface fluxes computed from climatological atmospheric data and bulk formulae. Results from this uncoupled oceanic run, which are taken as initial conditions for the coupled experiments discussed later, are extensively documented in el Mohajir (1997). At the end of this spin-up, the OGCM SST distribution presents some biases with the observed SST which can reach 1° locally. We have not studied the impact of these initial state errors on the coupled model behaviour. Because of the high sensitivity of the system to small SST anomalies in the near equatorial Pacific region (Neelin and Dijkstra 1995), it is possible that the oceanic initial state has some influence on the simulated tropical climate. However, we note that the tropical climate simulated by the LMD atmospheric model coupled to a totally different oceanic model, initialised by internal and surface Newtonian restoring to Levitus (1982) temperatures and salinities, has a similar behaviour to one described hereafter (Barthelet et al. 1998).

The atmospheric and the ocean-sea ice models are coupled at a one day frequency, which is the current time-step of the latter model. Fields are interpolated from one grid to the other by a procedure which preserves the average of the surface energy and water budget. In order to avoid mismatch problems between non-overlapping land masks, we have introduced fractional sub-grid continental and oceanic meshes in the LMD AGCM such that the World Ocean surface is exactly the same in both models. This enables conservation of extensive quantities exchanged between the models through a simple interpolation procedure. A 3-year simulation (acronym C_{CONT}) has been performed with the coupled model. Its results are described in the following section. Reasons for performing such short-term integrations will appear shortly as we present the amplitude of the SST drift and upheaval in the tropical atmospheric circulation, after just a few years of simula-

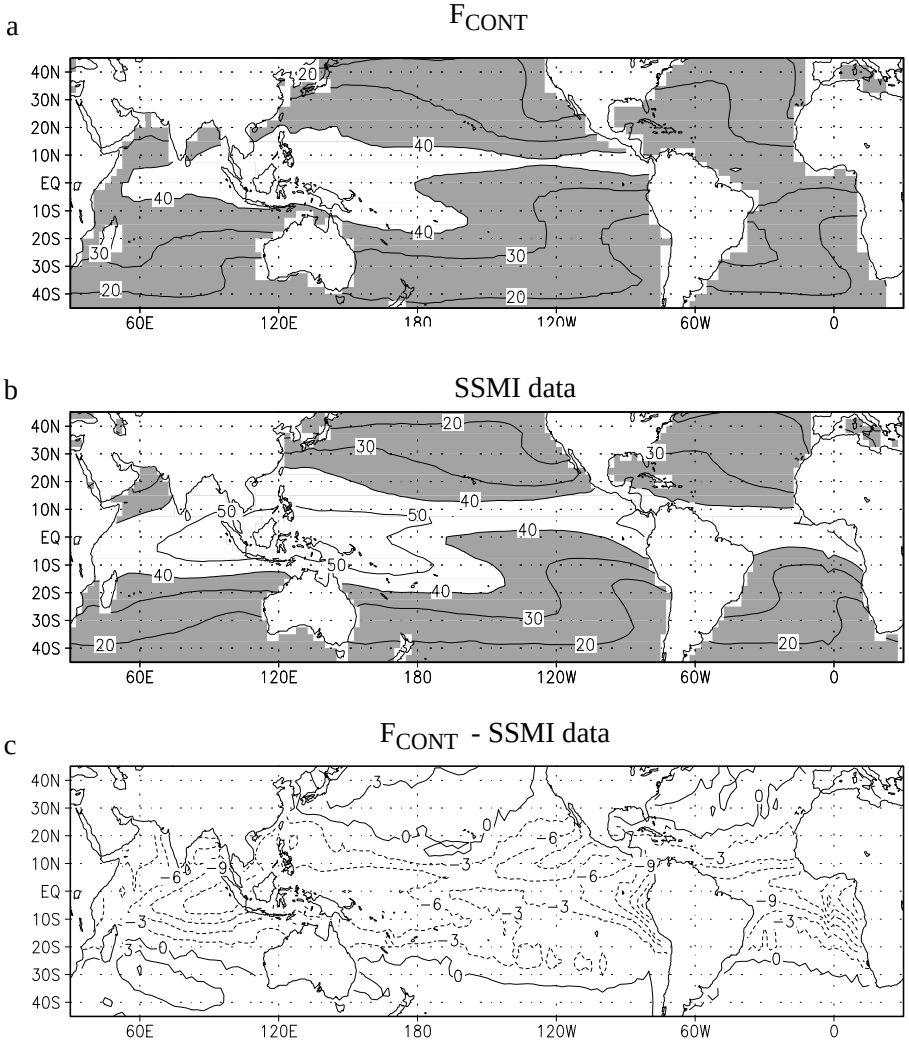

Fig. 3a–c Annual mean water vapour path (in kg/m^2) **a** diagnosed from the F_{CONT} simulation, **b** retrieved from satellite observations according to Wentz (1983) and **c** differences F_{CONT} − obervations

tion. Such a large amplitude lead us to believe that the coupled model response is not part of the model internal variability.

3 Analysis of the control coupled simulation

3.1 SST and troposphere

The first simulation with the LMD-CLIO AOGCM shows a pathological behaviour, which has been partly corrected in subsequent simulations. But this pathology, common to many models, although stronger in this first, non-flux corrected simulation, is the object of this study and deserves a careful analysis. A first approach to the model behaviour is obtained by a model-observation comparison of basin-averaged SST in the tropics (Fig. 5). The tropical Atlantic and Pacific Ocean share a similar cooling trend. By contrast, the Indian Ocean SSTs remain close to the observations. Inspection of geographical features (Fig. 6) confirms that the Atlantic and Pacific contain the main SST errors, which peak at −3 °C in the south Pacific, and −2 °C in the northern tropical Atlantic and Pacific. In most of the simulations carried out with AOGCMs, SSTs are too high along the western coastlines of the tropical landmasses. This warming, generally attributed to insufficient reflection of solar radiation by stratocumulus clouds (Meehl 1995), is present here in the eastern Atlantic but not in the eastern Pacific. In our simulation, the Pacific cold bias spans the whole basin and the Pacific warm pool has dramatically shrunk after only three years of simulation. A latitudinal average between 20°N and 20°S displayed in a time-longitude frame (Fig. 7) shows the continuous surface cooling trend in the Pacific Ocean. The cold anomalies seem to have their origins near the eastern border of the basin. One can identify a cooling signal peaking during the first part of each year, then propagating toward the central and western Pacific. By contrast to the Pacific cooling, a large pool of water where SSTs exceed 28 °C characterises the Indian Ocean (Fig. 6), which remains slightly warmer than in the observations. The Indonesian maritime continent may act as a dynamical barrier between the cold Pacific and the warm Indian Ocean.

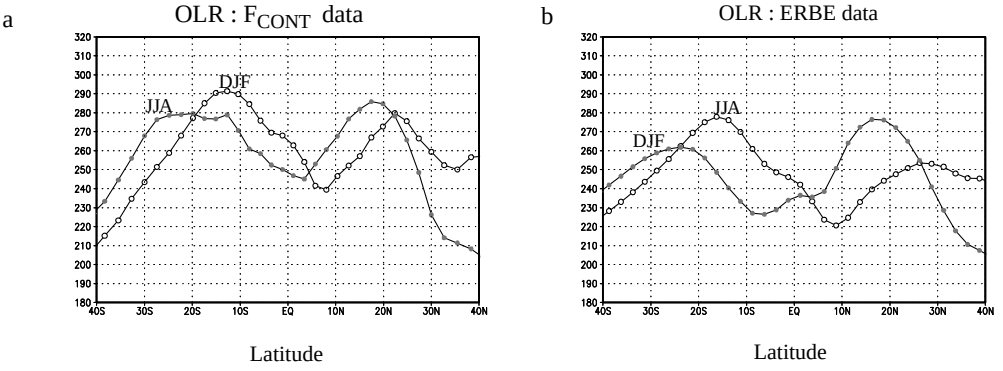

Fig. 4a, b Latitudinal distributions of the zonally averaged OLR at the top of the atmosphere **a** diagnosed from the F_{CONT} simulation **b** derived from ERBE measurements (Barkstrom and Smith 1986) for northern summer (*open circles*) and southern summer (*solid circles*). Units are Wm^{-2}. ERBE data is averaged over the 1985–1989 period and model data are averages over three years

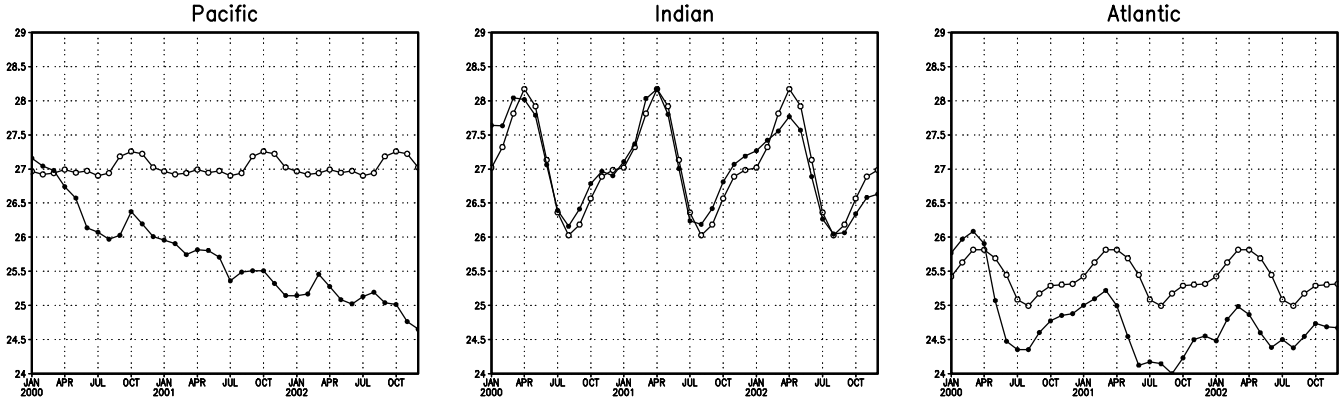

Fig. 5 Time series of the basin-averaged SST (°C) in the tropical Pacific, Indian and Atlantic Oceans from the C_{CONT} simulation (*solid circles*) and the mean climatological SST (*open circles*)

We now turn to the atmospheric response in terms of temperature, relative humidity and OLR. Difference in annual and zonal mean temperatures (computed as difference between the third year of integration of C_{CONT} and average over the whole F_{CONT} simulation) shows that the surface cooling in the tropics has been transferred to the lower part of the atmosphere (Fig. 8).

Above 750 hPa however, the atmosphere is slightly warmer at the end of the coupled simulation than it is during the uncoupled F_{CONT} experiment. The specific humidity has increased simultaneously in the upper troposphere (not shown), so that the relative humidity is larger, most notably in the near-equatorial region where the moistening reaches 10% (Fig. 9). This seems to express a paradox common to the SST changes observed throughout most of the tropics: as the tropical boundary layer gets drier and colder, one expects the static stability of the troposphere to increase, and deep convection, the main source of water vapour for the upper troposphere, to be less frequent, enforcing a drier troposphere. This raises the question of the location of high precipitating regions with the cooler SSTs. Plots of the SST fields and minimum in OLR fields (Fig. 10) show that convective activity over the western Pacific is limited to a thin band of latitude north of the equator. This region of lowest OLR seems located where the meridional SST gradient in the near-equatorial band is largest. We also note that the maximum in convective activity, over the western Pacific, is located roughly at the same location in summer and winter. By contrast, there is a seasonal cycle in convection over the Indian Ocean, as can be seen from the displacement of the low OLR minimum with the warmest SST and the low-level wind convergence zone (Fig. 10). Both in the Indian and Pacific Oceans, the low-level convergence at 850 hPa (not explicitly shown) and low OLR values correspond geographically. In the Indian Ocean, the large pool of warm water with no gradient constitutes a convergence zone for the lower troposphere wind. Throughout the Pacific, meridional SST gradients structure near-surface pressure gradients, low-level wind convergence, ascent and precipitation. This results in a zonalisation of convective precipitation (Fig. 10) over the whole Pacific. The way SST drives (parametrised) convection in the western and central Pacific, resembles the SST-convection interactions restricted to the eastern Pacific in the real system (Gutzler and Wood 1990). Although this constitutes an evident failure of this climate model, we examine the implications of such a zonalisation in convective activity for the tropical circulation and the radiative planetary budgets.

3.2 Dynamical adjustments of the Hadley circulation

In the convective regions, internal and latent energy is transformed into potential energy. Horizontal fluxes of these quantities are defined as:

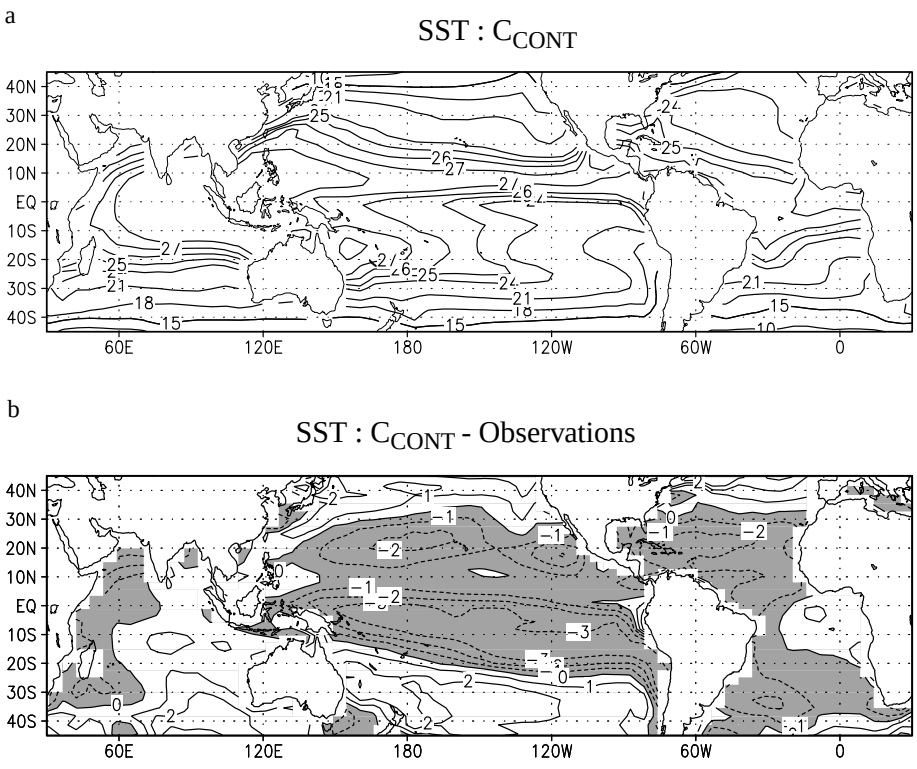

Fig. 6 a Annual mean SSTs from the C_{CONT} simulation (3rd year data) and **b** differences in annual mean SST between the C_{CONT} simulation and the observations of Levitus (1982)

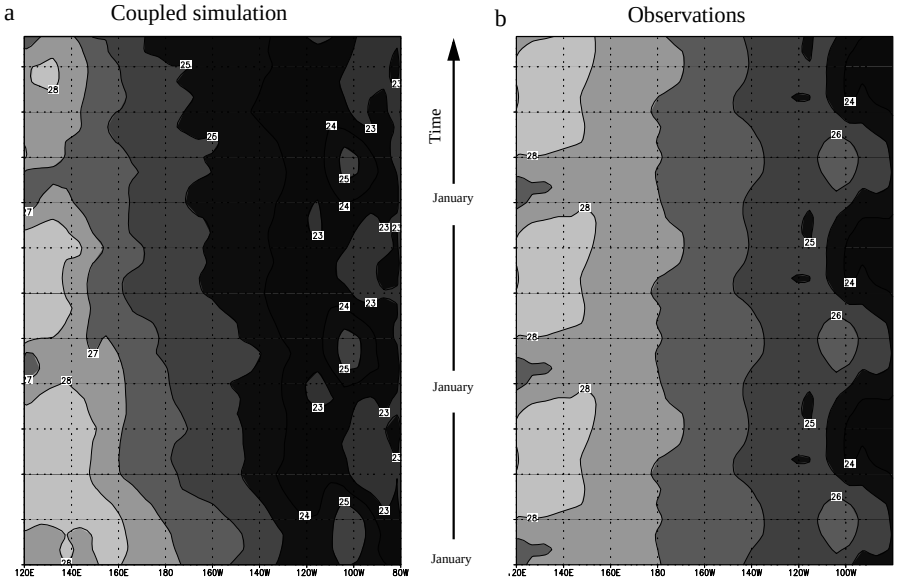

Fig. 7a, b Longitude-time plot of SST **a** in the C_{CONT} simulation **b** in the observations of Levitus (1982). The data has been averaged in latitude between 30°N and 30°S

$$F_{potential} = \rho g z \vec{V}\,\mathrm{d}z \quad (1)$$

$$F_{internal} = \rho C_p T \vec{V}\,\mathrm{d}z \quad (2)$$

$$F_{latent} = \rho L q \vec{V}\,\mathrm{d}z \quad (3)$$

where $\vec{V}$ is the horizontal wind, ρ is the air density, g is the acceleration due to gravity, z the altitude, C_pT is the sensible heat content and Lq the latent heat content. Taking a vertical average, and computing the horizontal divergence at each grid points of these fluxes, provides a measure of the energy conversion accomplished by the Hadley-Walker circulation (Polcher 1995). We show a zonal average performed over the Pacific Ocean domain of these quantities in Fig. 11. In accordance with previous diagnostics on OLR, we observe that the potential energy export in the Pacific region is concentrated near 8 to 10°N in the coupled simulation. It is more latitudinally spread around the equator, and less intense in the

forced simulation. Balancing for the increase in the divergence of $F_{potential}$, the convergence of $F_{internal} + F_{latent}$ is up to one and a half larger in C_{CONT}. This contrasts with the large decrease in the surface evaporation (Fig. 11c) following the SST drop, but the increase in the maximum of precipitation along the ITCZ. Acceleration of the circulation is necessary to explain the counter-intuitive adjustments of the surface heat fluxes on the one hand, and convergence of latent and internal energy on the other hand. This is confirmed by examining the changes in the meridional mass stream function (not shown), which show increase in the mass transport by the Hadley-Walker circulation between the forced and the coupled experiment. These results are coherent with those obtained in a number of theoretical studies, specifically devoted to computing the dynamics of the Hadley circulation as a response to a tropospheric heat source. Lindzen and Hou (1988) among others, have

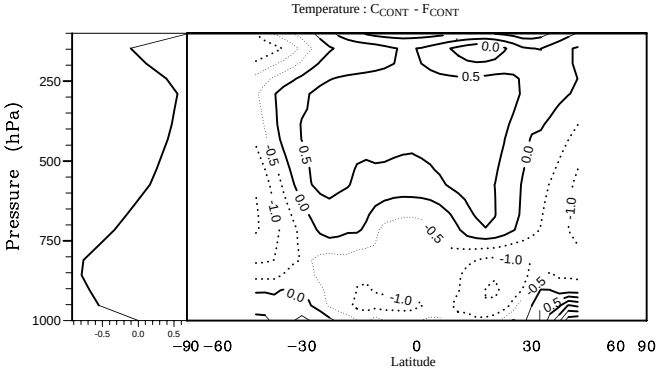

Fig. 8 Latitude-pressure distribution of the difference in annual mean absolute temperature between C_{CONT} (last year of simulation) and F_{CONT} (3-year average). The curve on the *left side* is the average over 45°S to 45°N

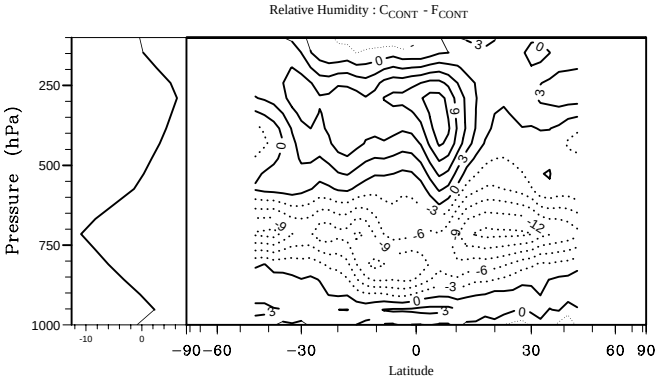

Fig. 9 Same as Fig. 8 except for relative humidity. Units are %

Fig. 10a, b Regions where the OLR is weaker than 250 Wm^{-2} (*in grey*), SST (*isolines*, in °C), and 850 hPa wind field (*vectors*, in ms^{-1}) from the third year of the C_{CONT} simulation for **a** JJA and **b** DJF

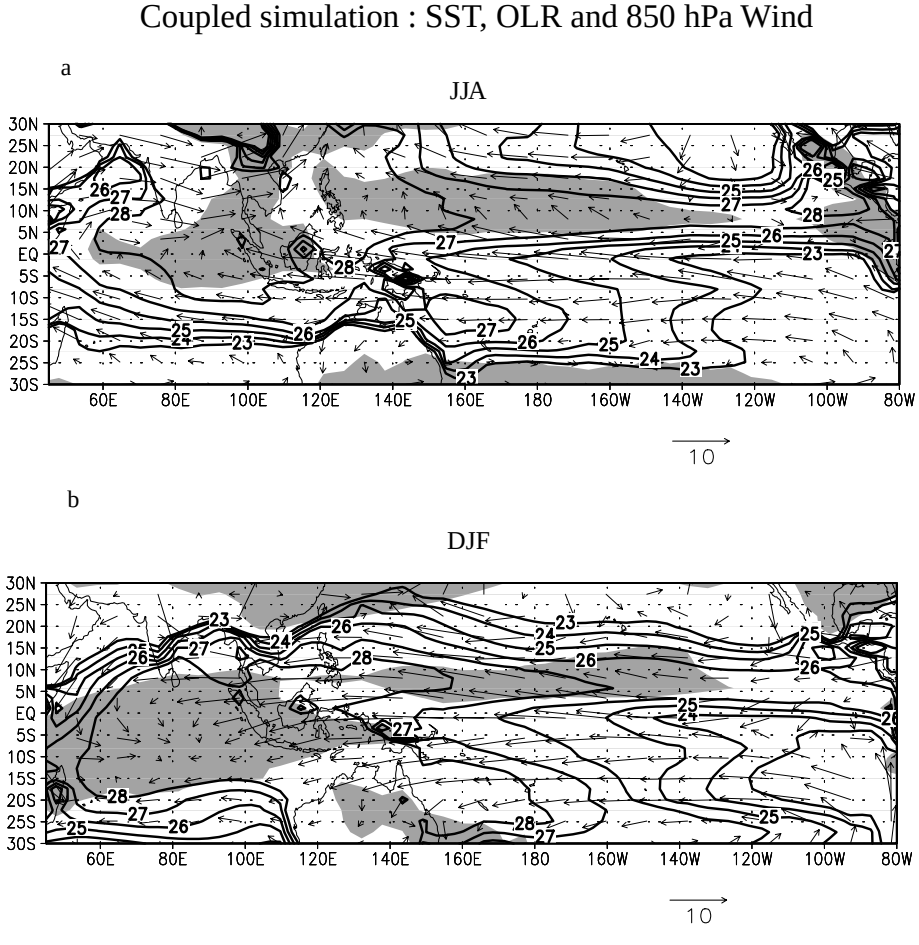

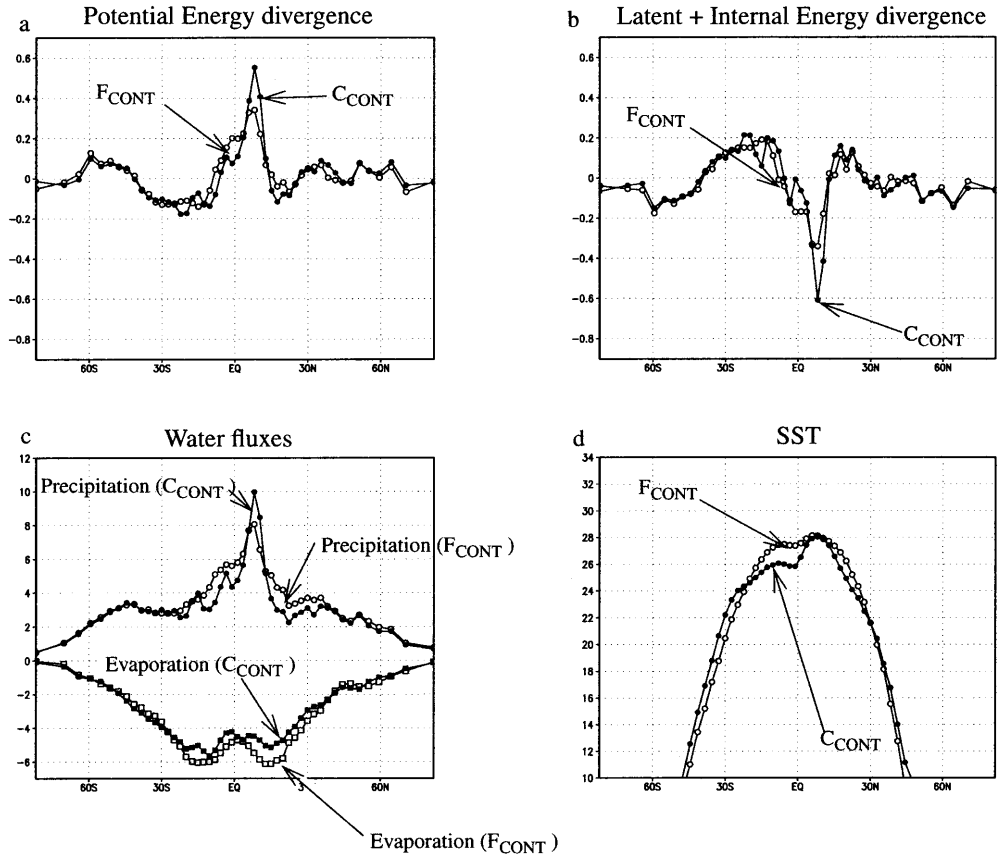

Fig. 11a–d Latitudinal distribution of the annual mean **a** potential energy divergence (kWm^{-2}), **b** latent plus internal energy divergence (kWm^{-2}), **c** surface precipitation and evaporation (mm/day), **d** SST (°C) averaged over the Pacific Ocean from 60° to 280°W, and derived from F_{CONT} (*open circles*) and C_{CONT} (*solid circles*) simulations. The quantities shown are three year averages

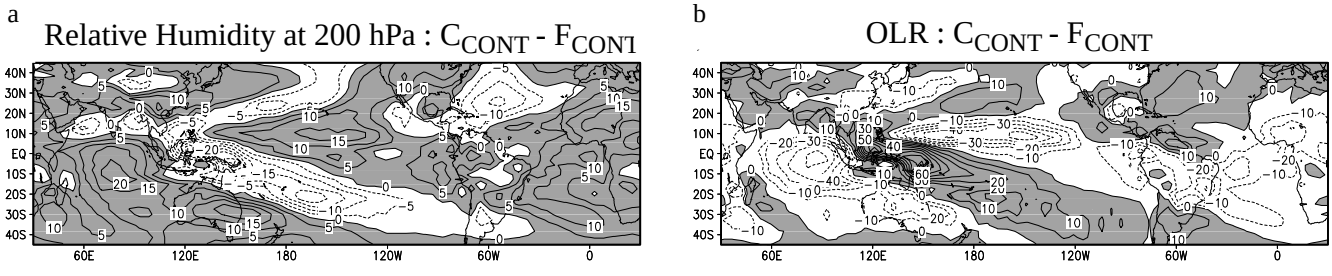

Fig. 12a, b Differences of annual mean **a** relative humidity at 200 hPa (%) and **b** OLR (Wm^{-2}) between experiments C_{CONT} and F_{CONT}. The data shown are 3-year averages

shown that the meridional circulation induced by a steady tropospheric heat source, is stronger when the heating is off the equator than centred on the equator. Similar conclusions were drawn by Numaguti (1993), after forcing an AGCM with SST distributions characterised by various zonal shapes in the tropical regions. This reflects the fact that the preferred latitudes for the oceanic precipitation zones are located off the equator (Waliser and Sommerville 1994).

In our coupled experiment, the large precipitation zones have moved off the equator because of a meridional SST gradient established slightly north of the equator. This meridional SST gradient is the result of the penetration of the cold tongue of water toward the western Pacific. As previously noticed, the latent heating remains at 8° to 10° north of the equator whatever the season. This steady heating re-enforces the "winter Hadley cell effect" (Lindzen and Hou 1988) in the coupled simulation. In summary, the SST-ITCZ configuration reached by the ocean-atmosphere system is a peculiar configuration for the tropical atmosphere circulation, since it enables greater efficiency of the Hadley cell thermal engine, with important radiative consequences for the planet: if the upper-tropospheric moistening sufficiently enhances trapping of LW radiation, such a SST-ITCZ configuration could induce a negative feedback on the surface cooling. We further analyse the simulation by evaluating the radiative feedbacks following (a) tropical Pacific surface cooling and (b) zonalisation of the convection in the tropical Pacific.

3.3 LW radiative budgets

Figure 12a shows that upper tropospheric moistening is well spread over most of the tropics and not limited to regions of deep convection, although they exhibit the largest sensitivity, as in the Indian and central Pacific Ocean. By contrast, the atmosphere over the south Pacific, which is no more convective, is considerably drier. It also radiates more LW energy to space, while the Indian and central Pacific regions trap up to 30 to 40 Wm^{-2} more LW radiation. The upper tropospheric moistening is not limited to the convective centres of action, probably because advection plays an important role in horizontally distributing the water vapour injected into the upper troposphere (Salathé and Hartmann 1997; Pierrehumbert and Roca 1999). For example, positive anomalies in relative humidity are found along 120°E from 20°S to 30°N, while convective activity is limited to a thin band of latitude in the equatorial Pacific (see Fig. 10). In the Atlantic region, one also notes a significant moistening of the upper troposphere, even over the ocean, while injection of moisture into the upper troposphere through deep convection is restricted to the southern American continent during the austral summer and the African continent in boreal summer (not shown). As discussed by Spencer and Braswell (1997), Salathé and Hartmann (1997), and Pierrehumbert and Roca (1999), upper-troposphere humidity (UTH) may considerably modify the radiative properties of the Earth, so we expect features shown in Fig. 12 to have a strong impact on the greenhouse effect.

On the other hand, the low and middle troposphere is much drier in the coupled experiment. Zonally averaged, the bias reaches 1 g/kg in the PBL. Differences in water vapour path between the C_{CONT} and the F_{CONT} simulation are shown in Fig. 13. Regions with negative anomalies (positive) are also regions with lower (higher) SST (see Fig. 6), reflecting the sensitivity of the vertically integrated water vapour path to PBL moisture content and SST. Dry anomalies reach 15 kg/m^2 over the climatological SPCZ, and remain considerable over the whole south Pacific Ocean. This tropospheric drying (it mainly reflects a PBL drying) is thermodynamically consistent with the surface cooling, since surface evaporation is smaller if surface temperatures are lower, through the surface evaporative cooling feedback (Hartmann and Michelsen 1993). In the drift out of equilibrium of our coupled model, what is the role of the water vapour feedback, and the UTH feedback on the surface and planetary LW cooling?

We have computed the greenhouse effect as $G = \epsilon \times SST^4 - OLR$. It represents the part of the LW radiation absorbed by the atmosphere and re-emitted toward the surface. One finds in the atmospheric greenhouse effect patterns the signature of the UTH (Fig. 14). Over the continental regions, the Indian and the Pacific Ocean convective regions, UTH increase is likely to be responsible for the increase in G. On both sides of the Pacific high precipitation zones, G is smaller in the coupled experiment. It is most likely driven by a drier lower troposphere, which generates a positive feedback on the SST cooling (Stephens 1990). The greenhouse effect feedback is negative (and of smaller amplitude) in a narrow band north of the equator, where convergence, uplift and heavy precipitation occurs exclusively. We draw two conclusions: first, as observed by Inamdar and Ramanathan (1995), the variability in the location of deep convection is a main source of variablity for the greenhouse effect in our simulation. Second, the drier troposphere enhances

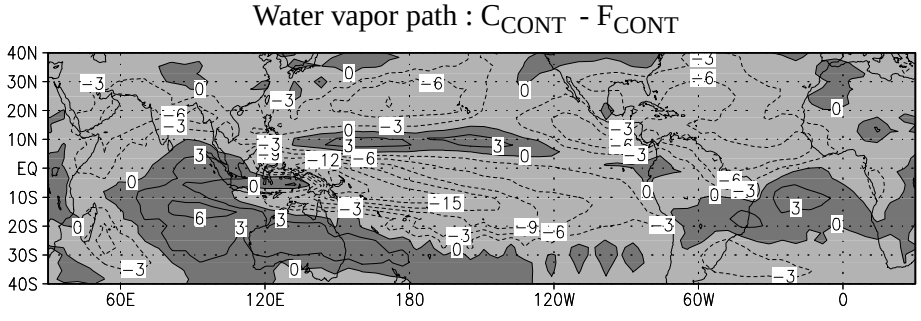

Fig. 13 Differences of annual mean vertically integrated water vapour between C_{CONT} and F_{CONT}, computed over the whole length of simulation. Units are kg/m^2

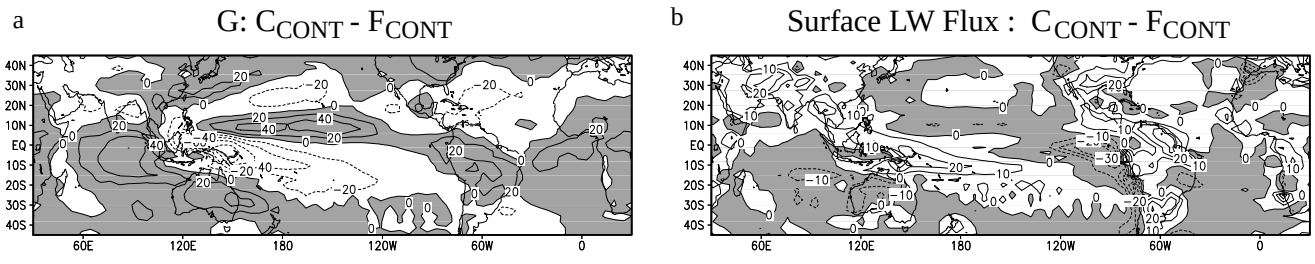

Fig. 14a, b Differences of annual mean **a** G (Wm^{-2}) and **b** net surface LW flux (Wm^{-2}) between the experiments C_{CONT} and F_{CONT}. The data shown are 3-year averages

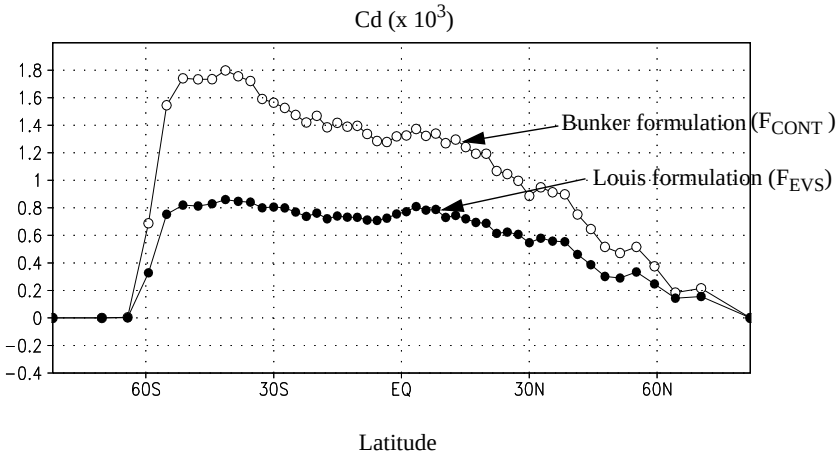

Fig. 15 Latitudinal distributions of the surface drag coefficient (multiplied by 1000) for boreal summer months from the F_{CONT} simulation (*open circles*) and the F_{EVS} simulation (*solid circles*)

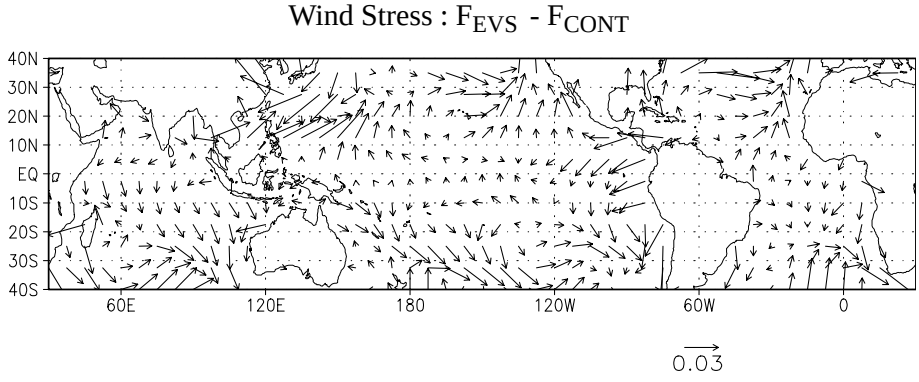

Fig. 16 Differences of annual mean surface wind stress between experiments F_{EVS} and F_{CONT}. The scale vector is 0.03 Nm^{-2}

planetary cooling over the oceanic deserts, despite increase in UTH over broad regions due to the zonalisation in the convection. Turning to the surface LW radiative budget (Fig. 14b), it appears that its sensitivity over most of the Pacific Ocean is also governed by the water vapour feedback. One exception is the far-east near equatorial Pacific, where the surface LW cooling decreases by 40 to 50 Wm^{-2}. We have related this to larger geographical extent of marine stratocumulus in the coupled simulation, because of a SST-Sc feedback discussed in more detail in the last section. The surface LW cooling is much smaller over regions which are covered by Sc, because the LW radiation divergence occurs at the cloud top.

In summary, our coupled model behaviour is therefore very unrealistic, but fully consistent. The surface cooling in the tropics reflects the excessive radiative loss of the atmosphere, its excessive dryness, despite the overestimated surface evaporation. At the same time, the zonal wind stress is overestimated, both in forced and coupled modes, and the meridional wind stress, in particular along the coastlines, is also too large. Many factors may induce errors in the surface turbulent fluxes: improper formulation of the PBL turbulent mixing, problems with the diabatic heating representation in convective regions, or parametrisation of the surface drag coefficient.

4 Sensitivity of the tropical air-sea interactions to surface drag parametrisation

The energy budget at the air-sea interface is a key process in the chain of interactions which affect the drift in the simulated climate. To test its importance, and decouple the role of atmospheric versus oceanic processes, we have carried out a sensitivity experiment to the parametrisation of the drag coefficient. The comparison of the forced and coupled experiments is especially useful. The forced simulation (hereafter referred to as F_{EVS}) of 3 year duration with prescribed climatological SST and sea ice extent, has been performed with the Louis et al. (1981) formulation for the drag coefficient. It is strictly parallel to the simulation F_{CONT}, in which the Bunker (1979) formulation is used. A seven year coupled experiment has also been conducted, referred to as C_{EVS}. The initial state and oceanic model version remain identical to those used in the C_{CONT} simulation. Over the oceans, the formulation proposed by Charnock (1955) for relating the roughness length to the surface friction velocity is used in computing the neutral drag coefficient, for both heat and momentum exchanges. The value of the "Charnock" constant used in this computation is 0.018. Results obtained from a three year average are compared with the data obtained from the F_{CONT} experiment. Figure 15 shows the zonal

profile of the drag coefficient for heat at the ocean surface diagnosed from the forced SST simulation. Values obtained in the sensitivity experiment are dramatically smaller than those computed with the Bunker (1979) formulation, and are significantly smaller than those found in the literature.

4.1 F_{EVS} compared to F_{CONT}

As expected, smaller values of C_d lead to a decrease in the amplitude of the surface wind stress over most of the oceanic domain (Fig. 16), despite an acceleration of the flow in the lower atmosphere (not shown). This decrease is particularly large in the eastern Pacific and Atlantic, close to the coastlines, but is weak over most of the central Pacific Ocean. In particular along the equator the impact is limited. We show on Fig. 17 differences in the various surface heat budget terms between the experiments F_{CONT} and F_{EVS}. The surface turbulent fluxes of latent and sensible heat have been added together to clarify the figure. In the zonal mean, they strongly decrease by 25 to 30 Wm^{-2} in the sub-tropical regions. This improves the model against the climatology. But the excessive coolness and dryness of the troposphere is enhanced (not shown). This deteriorates even more the thermodynamic structure of the model compared to the observations. The zonal structure of the total surface heat flux response closely follows that of the turbulent heat fluxes, but is slightly modified by changes in the surface radiative fluxes. Firstly, the amount of solar radiation available at the surface of the ocean is 5 Wm^{-2} larger, because of a slight decrease in PBL cloudiness. Second and more importantly, the net surface LW flux has increased by 15 Wm^{-2} between both experiments. This increase is due to a reduction in the downward LW radiation, induced by the drying of the troposphere (not shown). To summarise, two terms contribute mainly to the net heat flux sensitivity in the tropics: the turbulent surface fluxes and the downward LW flux. The LW sensitivity of water vapour is responsible for this greenhouse effect feedback.

4.2 C_{EVS} compared to C_{CONT}

4.2.1 Drift in the Pacific

In coupled mode, one sees from Fig. 18 that the tropical Pacific Ocean is slightly warmer (compared to C_{CONT}).

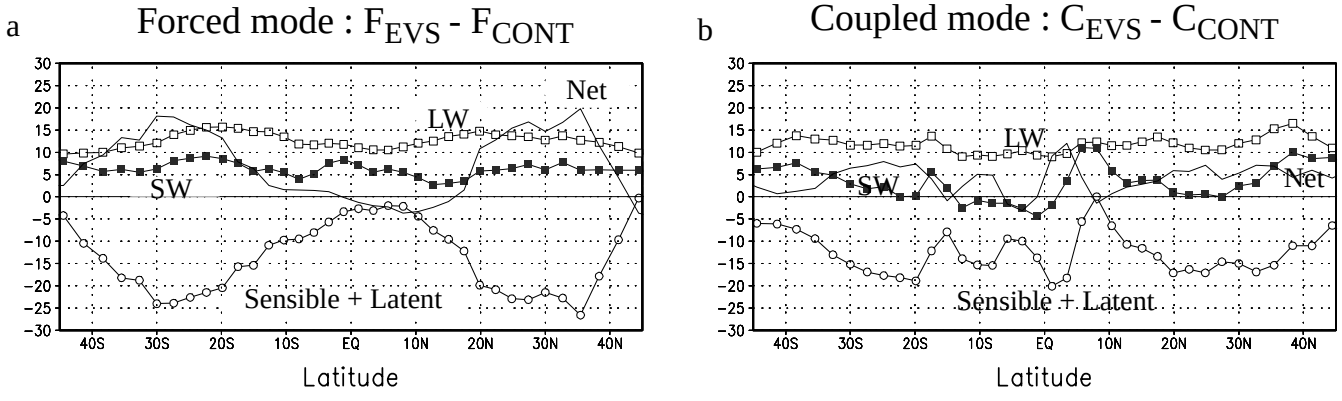

Fig. 17a, b Latitudinal distributions of the differences of latent and sensible heat flux (*open circles*), net LW flux (*open squares*), net shortwave radiation (*solid squares*) and total heat flux (*no symbol*) at the surface between experiments **a** F_{EVS} and F_{CONT} and **b** C_{EVS} and C_{CONT}. Units are Wm^{-2}, the data are 3-year averages

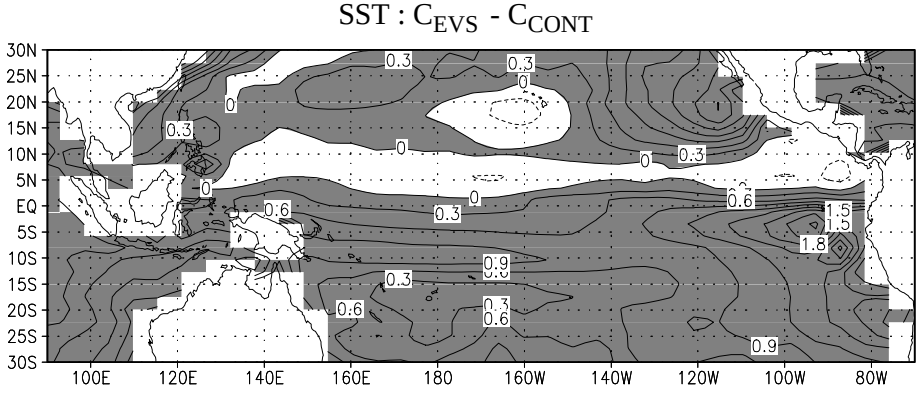

Fig. 18 Difference of annual mean SST over the tropical Pacific Ocean between experiments C_{EVS} and C_{CONT} after three years of simulation

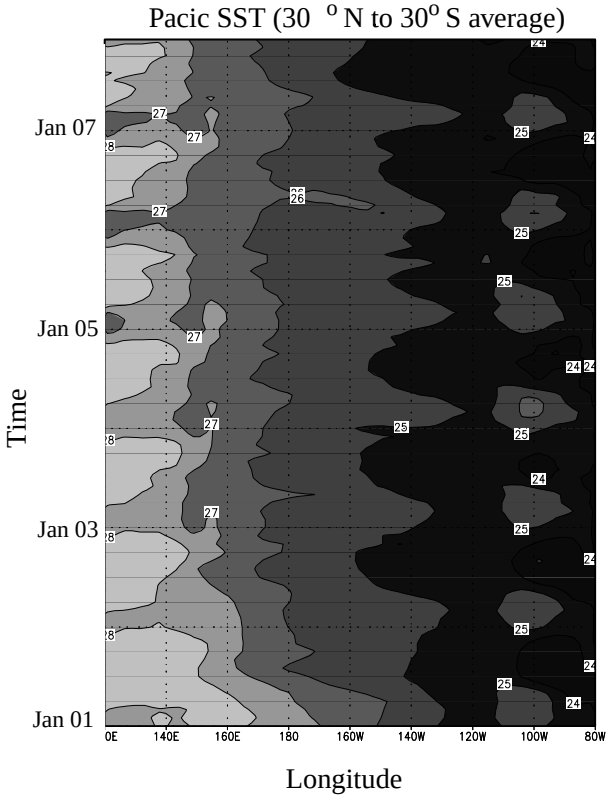

Fig. 19 Longitude-time cross-section of the SST averaged between 30°N and 30°S in the Pacific from the C_{EVS} simulation

The warming amplitude is moderate, except over the eastern Pacific where it reaches 2 °C. Time evolution of the SST field in the tropical Pacific (Fig. 19) shows interesting features occurring east of the dateline. SST in the eastern Pacific displays a seasonal cycle of small amplitude compared to the observed one (see Fig. 7), but whose timing looks reasonable. SSTs do not appear to drift toward increasingly cold temperatures along the coastlines, as was the case in the control experiment. But, although it is weaker than in the C_{CONT} experiment, the drift persists in the western Pacific. Therefore, some of the biases present in the previous experiment have been alleviated (namely the abrupt cooling over the eastern Pacific), while the general feature of the control experiment (namely tropical SSTs are generally too cold and the Pacific warm pool disappears) remain. With fixed SST, the main impact of using Louis et al.'s (1981) parametrisation for C_d was to decrease the surface turbulent fluxes and downward LW radiation. In coupled mode, these two terms also exhibit the largest sensitivity (see Fig. 17b). But, at least in the zonal mean, the cancellation between them is so pronounced that the impact on the net surface heat flux is small. The near-cancellation between the surface LW cooling term and the evaporative cooling term occurs because the latter is smaller in coupled mode than in forced mode (compare Fig. 17a, b). We have not quantified the relative role of changes in C_d, near-surface wind speed and stability in the surface layer, responsible for this reduced sensitivity. Qualitatively though, in forced mode, surface evaporation does not cool the surface. The surface evaporative cooling feedback is not operational, which explains why surface turbulent fluxes are more sensitive to modifications in the drag coefficient.

The SST sensitivity is weak and coherent with the idea that on a time scale of a few months or more, surface turbulent heat fluxes and atmospheric LW cooling are tightly coupled (Betts and Ridgway 1989). This is not to say that the parametrisation of surface drag is unimportant in AGCMs. It is important that the formulation be theoretically correct and validated against observations. But we suggest that, as long as the dry bias in the AGCM persists, along with positive biases in surface evaporation, the water vapour greenhouse effect will not be able to compensate for the surface evaporative cooling, thus driving a cold SST bias in the tropics. The overestimate in clear sky LW cooling, primarily balanced by large-scale subsidence, may also generate positive biases on zonal wind stress, with potential devastating effects on the oceanic mixed layer depth and equatorial upwellings. The coarse resolution of the oceanic model is a factor aggravating the AGCM deficiencies, since the small-scale oceanic equatorial dynamics can not be captured at a 3° resolution.

4.2.2 Importance of the cold tongue for the Pacific drift

Detailling terms in the surface heat budget over the eastern Pacific reveals that the SST warming signature (compared to C_{CONT}), is found in the absorbed solar radiation (Fig. 20a), which occurs concurrently with a smaller cloud fraction in the boundary layer (Fig. 20c, d). The decrease in cloud fraction itself is due to changes in the large-scale environment, since we have verified that the Sc cloud cover over the cold tongue was not sensitive to C_d in forced mode. There exists a feedback between SST (or PBL temperature) and boundary layer convective regime and cloudiness. Over warmer SST, the PBL is expected to be deeper and warmer with less stratiform cloudiness than over colder SST. Observational evidences for such a feedback is provided in the study by Klein and Hartmann (1993), while theoretical and modelling confirmation can be found in Bretherton and Wyant (1997). Although smaller values in subsidence may also contribute to the pattern seen in Fig. 20, it is likely that most of the impact on Sc extent comes from higher SST. In a shallow, relatively well-mixed PBL as is the case over the eastern Pacific, the temperature in the PBL should increase with the SST. This warming actually decreases the lower static stability, but the PBL model is probably not sophisticated enough to dynamically react to such changes in the inversion strength. Rather, we think that a simple decrease in relative humidity below the inversion explains the Sc cloud cover sensitivity to warmer SST. What provides

the original SST warming for this feedback to occur? Compared to C_{CONT}, the meridional wind stress along the Chile and Mexico coastlines is considerably reduced. This directly affects the coastal upwellings. In summary, the eastern Pacific warming follows from a combination of factors: reduction in surface friction, which by a mechanical effect on the ocean induces SST warming; itself leads to less stratiform cloudiness through a thermodynamical feedback; and a radiative feedback (decrease in planetary albedo) further warms the SST. The PBL and cloud parametrisations implemented in the model capture at least one aspect of the important positive feedback between low SST and high cloud fraction (Miller 1997), even if this occurs through a much simpler relative humidity effect, than through the complex set of feedbacks expected in reality (Bretherton and Wyant 1997).

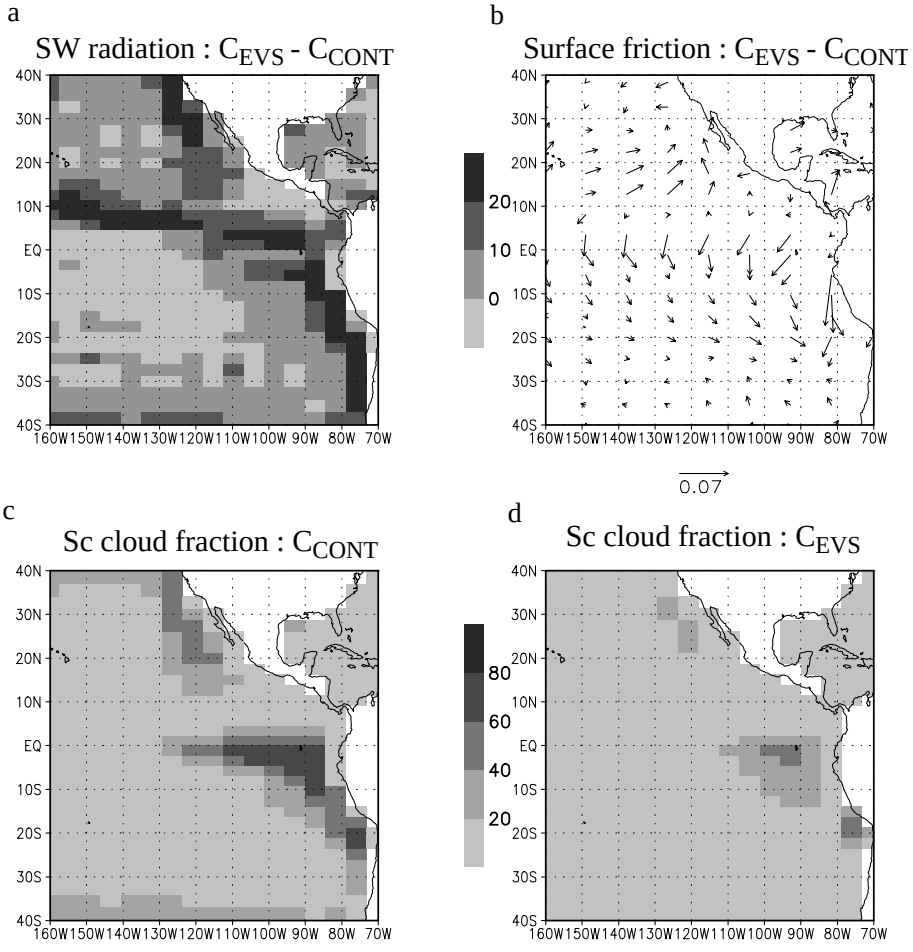

Fig. 20a–d Differences of annual mean **a** shortwave radiation absorbed at the surface (in Wm^{-2}) and **b** surface wind stress (Nm^{-2}) between the C_{EVS} and the C_{CONT} simulations in the eastern tropical Pacific. Annual mean cloud fraction (in %) for the **c** C_{CONT} and **d** C_{EVS} experiment

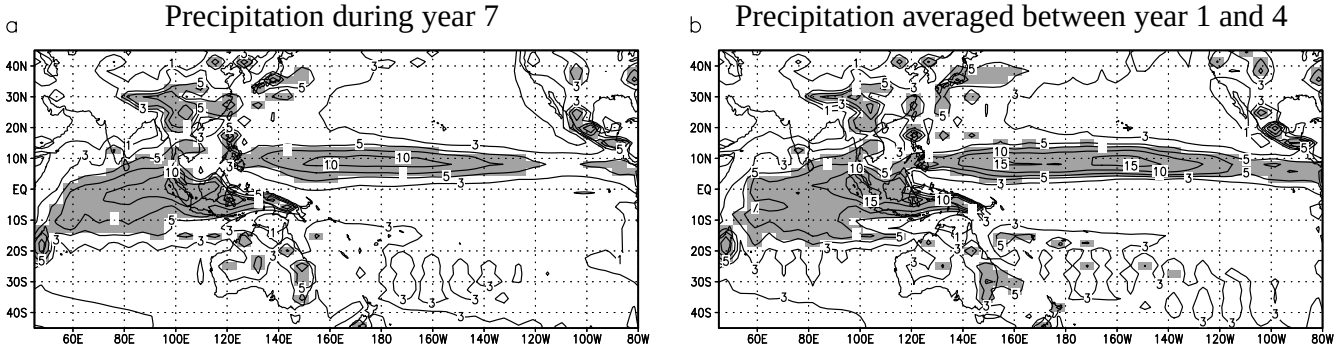

Fig. 21a, b Geographical distribution of the annual mean precipitation over the tropical Pacific **a** from the last year of the C_{EVS} simulation and **b** averaged over the first four years of the C_{EVS} simulation. Units are mm/day

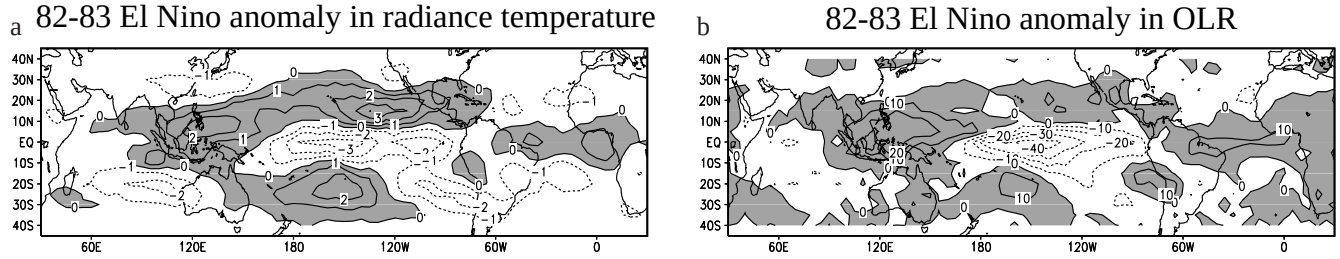

Fig. 22a, b Anomalies in **a** radiance temperature (K) and **b** OLR (Wm^{-2}) computed as differences between data averaged during the 1982–83 El Nino (from June, 1 1982 to May, 30 1983) and the 1975–1987 average

4.3 SST structure and water vapour feedback

Figure 21 shows the location of the high precipitation zones in the experiment C_{EVS}. Regions of high precipitation remain particularly stationary and zonally oriented in the Pacific during the whole simulation, much like in the C_{CONT} simulation. This off-equatorial locking of precipitation is likely to be occurring in any coupled model that simulates a near equatorial surface cooling, causing unrealistic meridional SST gradients. It is widely accepted that cloud and water vapour feedbacks are the most important processes for the climate sensitivity. We suggest that through its ability to control the position of the ITCZ, the oceanic circulation near the equator is an important property controlling the water vapour feedback. Turning our attention to observations, we will remark that during warm phase of ENSO, zonalisation of the convective activity is also clearly observed. Figure 22 shows anomalies in radiance temperature at 6.7 microns and OLR derived from satellite observations. Anomalies are computed as difference between the 1983 year, during which a strong positive phase of ENSO peaked, and the 1979–1988 period. In this channel, positive radiance temperature anomalies are significant indicators of negative anomalies in moisture content within the 500–200 hPa region (Salathé et al. 1995). In the central near-equatorial Pacific where convection did migrate during the warm phase of ENSO, one finds positive UTH anomalies and negative dry anomalies surrounding this region. OLR anomalies for the same period reach 30 Wm^{-2} (or 10 Wm^{-2}) over the moister (or drier) areas. Comparison of Fig. 22 and 12 is striking. It illustrates that the equatorial oceanic circulation can have a strong impact on the water vapour feedback through its control of the ITCZ position. In the real system, two regimes of SST-greenhouse effect relationships must be distinguished. One regime is thermodynamically triggered by the SST value, the other one dynamically triggered by the SST distribution (e.g., Lau et al. 1997). AGCM forced by observed SST, as Soden (1997) has shown for the GFDL model can capture these two regimes. But to what extent these SST-greenhouse feedbacks are properly captured by coupled atmosphere-ocean models, will depend on the ability of the oceanic model to realistically structure the SST in the near equatorial region.

5 Summary and conclusions

We have discussed simulations conducted with a global AOGCM, limiting the analysis to the tropics, and focusing on the role of atmospheric processes in the SST distribution upheaval. The control coupled simulation is characterised by a strong and continuous cooling in the tropical Pacific, a moderate cooling in the Atlantic and a relatively realistic SST pattern in the Indian Ocean. In our analysis we have focused on the tropical Pacific SST which presents the largest discrepancies with observations. The pronounced Pacific cooling is accompanied by a reduction in the size of the convective areas, and in the surface evaporation amplitude over the tropical oceans. Convection is restricted to the Indian Ocean and to a thin band of latitude north of the equator, spanning the whole tropical Pacific Ocean. We find that the tropical SST drift is coherent with an unrealistically intense hydrological cycle simulated by the AGCM, driven or caused by excessive planetary LW cooling. Despite these energetic imbalances, which reveal flaws in the parametrisations affecting the hydrological cycle, we have analysed in detail the ocean-atmosphere feedbacks resulting from the penetration of the cold tongue toward the western Pacific. With the convection schemes used in the AGCM (a combination of Manabe and Kuo schemes), the near-equatorial cold tongue triggers a quasi-stationary pattern of precipitation in the entire Pacific, by controlling large-scale convergence of humid air in the PBL. The locking of low-level and off-equatorial, uplift motion in the Pacific, is responsible for moistening the upper-troposphere through the prognostic liquid water statistical scheme. The subsidence zones are drier, extend over broader areas in the coupled simulation, and the greenhouse effect amplifies the SST cooling over the Pacific region.

The atmospheric dynamical and radiative feedbacks at work in the simulated atmosphere-ocean system, illustrate that the oceanic circulation near the equator, by structuring the SST field, can not be ignored in sensitivity studies of the climate. As pointed out by Vintzeleos et al. (1999) and Périgaud et al. (1997), the oceanic circulation in the near-equatorial band constitutes a component of the coupled ocean-atmosphere system that models need to reproduce properly,

because of the coupling through Ekman dynamics between the sub-surface equatorial currents and the ITCZ. This may require higher spatial resolution than currently used in the oceanic component of climate models. Therefore, when interpreting climatic scenarios obtained with 3D models, one must be aware that water vapour and cloud feedbacks are sensitive to near equatorial oceanic dynamics. Another conclusion is drawn from a sensitivity experiment performed with a different formulation of the surface drag coefficient. We attribute to a feedback between SST and Sc cloud cover (Klein and Hartmann 1993) a large part of the eastern Pacific drift, suppressed with the Louis' et al.'s (1981) parametrisation for the drag coefficient which provides lower values of the meridional wind stress along the coastlines. Despite these large improvements, that we attribute mostly to local processes occurring in the eastern Pacific, the major deficiencies of the simulation remain unchanged. This suggests that these problems are more constrained by the heat budget at the top-of-the-atmosphere than by details of the surface flux parametrisation. This means that any new parametrisation aiming at an improvement of the surface heat budget, should simultaneously improve the TOA heat budget in order to have some positive impact on the coupled model behaviour.

Acknowledgements Many thanks are due to Prof R. Sadourny for providing Université Catholique de Louvain with the LMD General Circulation Model. H. G. is indebted to Prof D. L. Hartmann and C. S. Bretherton for providing support necessary to complete this manuscript. T. F. is a Research Associate at the National Fund for Scientific Research (Belgium). This work was done within the scope of the Global Change and Sustainable Development Program (Belgian State, Prime Minister's Services, Federal Office for Scientific, Technical and Cultural Affairs, contract CG/DD/09A), the Concerted Research Action 092/97-154 (French Community of Belgium, Department of Education, Research and Formation), and the Environment and Climate Program (European Commission, contract ENV4-CT95-0102). All of this support is gratefully acknowledged.

References

Barkstrom BR, Smith GL (1986) The Earth Radiation Budget Experiment: science and implications. Rev Geophys 24: 379–390

Barthelet P and 25 co-authors (1998) Simulations couplées globales des changements climatiques associés à une augmentation de la teneur atmosphérique en CO_2. C R Acad Sci Paris 326: 677–684

Betts AK, Ridgway W (1989) Climate equilibrium of the atmospheric convective boundary layer over a tropical ocean. J Atmos Sci 46: 2621–2641

Boer GJ, Mc Farlane NA, Laprise R, Henderson JD, Blanchet J-P (1984) The Canadian Climate Centre spectral atmospheric general circulation model. Atmos-Ocean 22: 397–429

Bretherton CS, Wyant MC (1997) Moisture transport, lower static stability, and decoupling of cloud-topped boundary layers. J Atmos Sci 54: 148–167

Bunker AF (1979) Computation of surface energy flux and annual air-sea interaction cycles of the North Atlantic Ocean. Mon Weather Rev 104: 1122–1140

Charnock H (1955) Wind stress on a water surface. Q J R Meteorol Soc 81: 639–651

Clement A, Seager R, Cane MA, Zebiak SE (1996) An ocean dynamical thermostat. J Clim 9: 2190–2196

Deleersnijder E, Campin J-M (1995) On the computation of the barotropic mode of a free-surface World Ocean model. Ann Geophys 13: 675–688

Ducoudré NI, Laval K, Perrier A (1993) SECHIBA, a new set of parametrisations of the hydrologic exchanges at the land/atmosphere interface within the LMD Atmospheric General Circulation Model. J Clim 6: 248–273

Fichefet T, Morales Maqueda MA (1997) Sensitivity of a global sea ice model to the treatment of ice thermodynamics and dynamics. J Geophys Res 102: 12609–12646

Fouquart Y, Bonnel B (1980) Computations of solar heating of the Earth's atmosphere: a new parametrisation. Beitr Phys Atmos 53: 35–62

Gleckler PJ, Weare BC (1997) Uncertainties in global ocean surface heat flux climatologies derived from ship observations. J Clim 10: 2764–2781

Goosse H, Campin J-M, Fichefet T, Deleersnijder E (1997a) Sensitivity of a global ice-ocean model to the Bering Strait throughflow. Clim Dyn 13: 349–358

Goosse H, Campin J-M, Fichefet T, Deleersnijder E (1997b) Impact of sea-ice formation on the properties of Antarctic Bottom Water. Ann Glaciol 25: 276–281

Gutzler DS, Wood TM (1990) Structure of large-scale convective anomalies over tropical oceans. J Clim 3: 483–496

Hartmann DL, Michelsen ML (1993) Large-scale effects on the regulation of tropical sea surface temperatures. J Clim 6: 2049–2062

Harzallah A, Sadourny R (1995) Internal versus SST-forced atmospheric variability as simulated by an atmospheric general circulation model. J Clim 8: 474–495

Inamdar AK, Ramanathan V (1994) Physics of greenhouse effect and convection in warm oceans. J Clim 7: 715–731

Johnson DR (1997) General coldness of climate models and the second law: implications for modeling the Earth system. J Clim 10: 2826–2846

Klein SA, Hartmann DL (1993) The seasonal cycle of low stratiform clouds. J Clim 6: 1587–1606

Kuo HL (1965) On the formation and intensification of tropical cyclones through latent heat release by cumulus convection. J Atmos Sci 22: 40–63

Larson K, Hartmann DL, Klein SA (1999) On the role of clouds, water vapor, circulation and boundary layer structure in the sensitivity of the tropical climate. J Clim 12: 2359–2374

Lau K-M, Wu HT, Bony S (1997) The role of large-scale atmospheric circulation in the relationship between tropical convection and sea surface temperature. J Clim 10: 381–392

Le Treut H, Li ZX (1988) Using Meteosat data to validate a prognostic cloud generation scheme. Atmos Res 21: 273–292

Le Treut H, Li ZX, Forichon M (1994) Sensitivity of the LMD general circulation model to greenhouse forcing associated with two different cloud water parametrisations. J Clim 7: 1827–1840

Levitus S (1982) Climatological Atlas of the World Ocean. NOAA Prof Pap 13, US Government Printing Office, Washington, DC, USA

Lindzen RS, Hou AY (1988) Hadley circulation for zonally averaged heating centered off the equator. J Atmos Sci 45: 2416–2427

Louis JF, Tiedtke M, Geleyn JF (1981) A short history of the PBL parametrisation at ECMWF. Proc Workshop on Boundary Layer Parametrisation, ECMWF, Reading, 59–79.

Ma C-C, Mechoso CR, Arakawa A, Farrara JD (1994) Sensitivity of a coupled ocean-atmosphere model to physical parametrisations. J Clim 7: 1883–1896

Ma C-C, Mechoso CR, Robertson AW, Arakawa A (1996) Peruvian stratus clouds and the tropical Pacific circulation: a coupled ocean-atmosphere GCM study. J Clim 9: 1635–1645

Manabe S, Smagorinski J, Strickler RF (1965) Simulated climatology of a general circulation model with a hydrological cycle. Mon Weather Rev 93: 768–798

Meehl GA (1995) Global coupled general circulation models. Bull Am Meteorol Soc 76: 951–957

Meehl GA, Wahington WM (1995) Cloud albedo feedback and the super greenhouse effect in a global coupled GCM. Clim Dyn 11: 399–411

Miller RL (1997) Tropical thermostats and low cloud cover. J Clim 10: 409–440

Mitchell TP, Wallace JM (1992) The annual cycle in equatorial convection and sea surface temperature. J Clim 5: 1140–1156

el Mohajir M (1997) Elaboration d'un modèle global tri-dimensionnel atmosphère-océan-glace marine en vue d'applications climatiques: validation de la composante oceéan – glace marine. PhD thesis, Univeristé Catholique de Louvain, Faculté des Sciences, Louvain-la-Neuve, Belgium

Morcrette J-J (1991) Radiation and cloud radiative properties in the European Center for Medium-Range Weather Forecasts forecasting system. J Geophys Res 96: 9121–9132

Neelin JD, Dijkstra HA (1995) Ocean-atmosphere interactions and the tropical climatology. Part I: the dangers of flux corrections. J Clim 8: 1325–1342

Numaguti A (1993) Dynamics and energy balance of the Hadley circulation and the tropical precipitation zones: significance of the distribution of evaporation. J Atmos Sci 50: 1874–1887

Pacanowski RC, Philander SGH (1981) Parametrisation of vertical mixing in numerical models of tropical oceans. J Phys Oceanogr 11: 1443–1451

Périgaud C, Zebiak SE, Mélin F, Boulanger J-P, DeWitte B (1997) On the role of meridional wind anomalies in a coupled model of ENSO. J Clim 10: 761–773

Pierrehumbert RT (1997) Radiator fins and the local runaway greenhouse effect. J Atmos Sci 52: 1784–1806

Pierrehumbert RT, Roca R (1998) Evidence for control of Atlantic sub-tropical humidity by large scale advection. Geophys Res Lett 25: 4537–4540

Polcher J (1995) Sensitivity of tropical convection to land-surface processes. J Atmos Sci 52: 3142–3161

da Silva AM, Young CC, Levitus S (1995) Atlas of marine surface data, vol 2. US Government Printing Office, Washington DC, USA

Sadourny R, Laval K (1984) January and July performance of the LMD general circulation model. A Berger (Ed) Elsevier, Amsterdam, pp 173–198

Salathé EPJ, Hartmann DL (1997) A trajectory analysis of tropical upper-tropospheric moisture and convection. J Clim 10: 2533–2547

Salathé EPJ, Chesters D, Sud YC (1995) Evaluation of upper-tropospheric moisture climatology in a general circulation model using TOVS radiance observations. J Clim 8: 2404–2414

Sausen R, Barthel K, Hasselman K (1988) Coupled ocean-atmosphere models with flux corrections. Clim Dyn 2: 145–163

Soden BJ (1997) Variations in tropical greenhouse effect during El Nino. J Clim 10: 1050–1055

Spencer RW, Braswell WD (1997) How dry is the tropical free troposphere? Implications for global warming theory. Bull Am Meteorol Soc 78: 1097–1106

Stephens GL (1990) On the relationship between water vapor over oceans and sea surface temperature. J Clim 3: 634–645

Terray L (1998) Sensitivity of climate drift to atmospheric physical parametrisations in a coupled ocean-atmosphere general circulation model. J Clim 11: 1633–1658

Vintzeleos A, Delecluse P, Sadourny R (1999) On the mechanisms in a tropical ocean-global atmosphere coupled general circulation model. Part I: mean state and the seasonal cycle. Clim Dyn 15: 43–62

Waliser AJ, Sommerville RCJ (1994) Preferred latitudes of the Intertropical Convergence Zone. J Clim 51: 1619–1639

Wentz X (1983) A model function for ocean microwave brightness temperatures. J Geophys Res 88: 1892–1908

Xu K-M, Randall DA (1996) Evaluation of statistically based cloudiness parametrisations used in climate models. J Atmos Sci 53: 3103–3119

Zhang GJ, Ramanathan V, McPhaden MJ (1995) Convection-evaporation feedback in the equatorial Pacific. J Clim 8: 3084–3090